

Variability in the mesosphere observed by the Nimbus 6 pressure modulator radiometer

Bryan N. Lawrence¹

Space Sciences Division, Rutherford Appleton Laboratory, Didcot, England, U.K.
Department of Physics, University of Oxford, Oxford, England, U.K.

William J. Randel

National Center for Atmospheric Research, Boulder, Colorado

Abstract.

The pressure modulator radiometer flew aboard Nimbus 6, collecting radiance data from June 1975 until June 1978. These data have been processed to yield daily temperatures, geopotential heights, and balance wind estimates from the stratosphere and mesosphere (30–85 km) for the entire period. We use these data to examine the variability of both the zonal-mean and the nonzonal disturbances present in the data. In terms of the zonal-mean, we show that the COSPAR International Reference Atmosphere (1986), developed from these data, can be misleading in the mesosphere due to the underlying interannual variability and the merging with other data sets. Daily variability of the zonal-mean flow is examined, and these data show strong evidence of coupling between the stratosphere and mesosphere for such variations. We also find evidence for significant coupling of wave-like events in the stratosphere and the mesosphere but that not all such disturbances seen in the mesosphere are due to simple propagation from below. Space-time spectral analysis is used to search for traveling planetary waves: Results show a weak 5-day normal mode present in the equinox seasons, which appears to correspond to the first symmetric mode predicted by theory. These data also show clear evidence of the 4-day wave in all three southern winters examined and are consistent with the hypothesis that this mode grows due to instability of the background zonal flow.

1. Introduction

Since the advent of satellite instrumentation for remote sounding of the middle atmosphere, there have been many generations of instruments and retrieval techniques. In the stratosphere, data acquisition has proceeded from scientific experimentation (for example, the early selective chopper radiometer (SCR) instruments aboard Nimbus 3 and later satellites) to the production of standard meteorological data (for example, the stratospheric sounding unit (SSU) instruments aboard the NOAA series of satellites). However, prior to the Upper Atmosphere Research Satellite (UARS) the mesosphere has only been sampled extensively by four instruments: the pressure modulator radiometer (PMR) aboard Nimbus 6, the limb infrared monitor of

the stratosphere (LIMS) and the stratosphere and mesosphere sounder (SAMS) instruments aboard Nimbus 7; and the ultraviolet spectrometer aboard the Solar Mesospheric Explorer (SME). Of these instruments, only the PMR provided global daily coverage of the mesosphere during all seasons.

The data from the PMR provide an excellent context for interpreting measurements from the UARS in terms of the typical structure and variability of the mesosphere. Although the instrument flew nearly 20 years ago, the data have not yet been fully analyzed. In this study, we review the typical zonal-mean temperature structure of the mesosphere and highlight some aspects of mesospheric interannual variability by contrasting it with the COSPAR International Reference Atmosphere (1986) (CIRA86) [Fleming *et al.*, 1990] climatology [Barnett and Corney, 1985]. We then examine the temporal variability of both the zonal-mean and the eddy components in these data.

Before proceeding, it is important to recall that the Nimbus 6 PMR was a nadir instrument with very deep vertical weighting functions [Curtis *et al.*, 1973; Labitzke and Barnett, 1981]. The effect of such broad weighting functions is both to select only phenomena with

¹Department of Physics and Astronomy, University of Canterbury, Christchurch, New Zealand

large vertical scales and to underestimate the amplitude of any perturbations associated with such phenomena, particularly in the upper mesosphere. Because the raw data collected were radiance, the further retrieval of temperature generally introduced yet more smoothing of the real atmospheric perturbations via the introduction of the retrieval climatology.

Early analyses of these data focused on temperature retrievals of monthly means and a limited set of days. These monthly mean data provided the basis for the mesospheric section of the CIRA86 climatology and of the extended diagnostics of *Marks* [1989]. (Actually, for the heights we are interested in, CIRA86 is based on an earlier climatology, that of *Barnett and Corney* [1985], who combined PMR data with SCR data.) Subsequently, the entire PMR data set (from mid-June 1975 until the middle of June 1978) has been reretrieved by Clive Rodgers (Oxford University) to provide daily along-track profiles of temperatures throughout the stratosphere and mesosphere. These profiles have been gridded by John Gille and Dan Packman at the National Center for Atmospheric Research using a Kalman filter algorithm to provide daily estimates of zonal-mean and zonal waves 1-6 on a 4° latitude grid over 80°S to 80°N . The true vertical resolution of the retrievals is probably in excess of 15 km, although they have been oversampled to provide a vertical grid at 3.5-km intervals. The resulting data are the subject of this study.

Above 80 km, our results should be assessed with caution, since although the data was retrieved with a correction for nonlocal thermodynamic equilibrium (non-LTE), there are now some questions as to whether the influence of non-LTE on temperature retrievals is as great as was expected at the time of calculation. This means that at some of the higher altitudes where the assumption may have been in error, the mean temperatures may have been underestimated especially near the cold summer mesopause (C. Rodgers, *personal communication*, 1995). It should also be noted that due to the configuration of the weighting functions, there is no real height discrimination in the lower and middle stratosphere. However, the temperature thickness of this region is well captured by the lower weighting functions.

Although the instrument collected data for the entire period from June 1975 until June 1978, there was a period of about 9 months (from October 1975 until July 1976) when the top sounding channel was not scanning correctly, leading to poor height discrimination (J. Barnett, *personal communication*, 1995). Accordingly, some of the data from this period probably further underestimate the true variability in the data, and we focus away from this time period for detailed studies.

Geopotential fields have been calculated from the PMR temperatures using the hydrostatic equation to stack temperature thicknesses on a boundary geopo-

tential field. The normal procedure to follow would be to take boundary fields from a suitable meteorological analysis or those derived from another instrument. However, for the PMR data, this was not possible, as contemporaneous global lower stratospheric analyses were not available. Accordingly, where we present time series of geopotential data, we have simply stacked the data upon a monthly mean 50-hPa field from a 12-year (1979-1990) climatology of National Meteorological Center (NMC) stratospheric analyses [*Randel*, 1992].

In addition, we were able to produce zonal-mean zonal winds using the gradient wind approximation. This approximation provides winds which are in excellent agreement with observations throughout the stratosphere. In the mesosphere, the gradient wind approximation is probably still a good measure of the zonal-mean zonal wind in the extratropics but not in the tropics. The tropical winds shown are simple interpolations between 15°N and 15°S .

2. The Mean State

In this section, we review three aspects of the zonal-mean view of the mesosphere. We first examine the interannual variability of the January monthly mean temperature fields in order to highlight the differences obscured by the averaging process inherent in making a climatology. Second, we show that when individual years are examined, the separated stratopause is more prominent in the northern hemisphere than hitherto suggested. Finally we show the seasonal evolution of the zonal wind, partly in order to show the background upon which we see large wave events and partly to demonstrate typical examples of evolution for later comparison with middle atmosphere models.

2.1. Zonal-Mean Temperatures

Monthly mean zonal-mean temperature sections from the three individual PMR years for January are displayed along with the resulting CIRA86 temperatures in Figure 1. It is worth restating here that the very cold summer mesopause is probably exaggerated in these data (the individual years, and the climatology), since all the retrievals assumed non-LTE in the upper mesosphere. The main features of the typical temperature structures shown here are described elsewhere [e.g., *Andrews et al.*, 1987]. Although it is not obvious from these figures, differences from the CIRA86 climatology demonstrate that for January, the CIRA86 atmosphere underestimates the northern hemisphere (NH) midlatitude temperatures in the region 60-80 km by 5-10 K in all years. By contrast, in the tropics, the lower regions (50-60 km) are overestimated by CIRA86 and the region 60-80 km underestimated, in both cases by 5-10 K. Examination of the differences for other months and years suggests that the differences can be up to 10° of either sign and are not simply due to interannual variability, but probably rather that the CIRA86 cli-

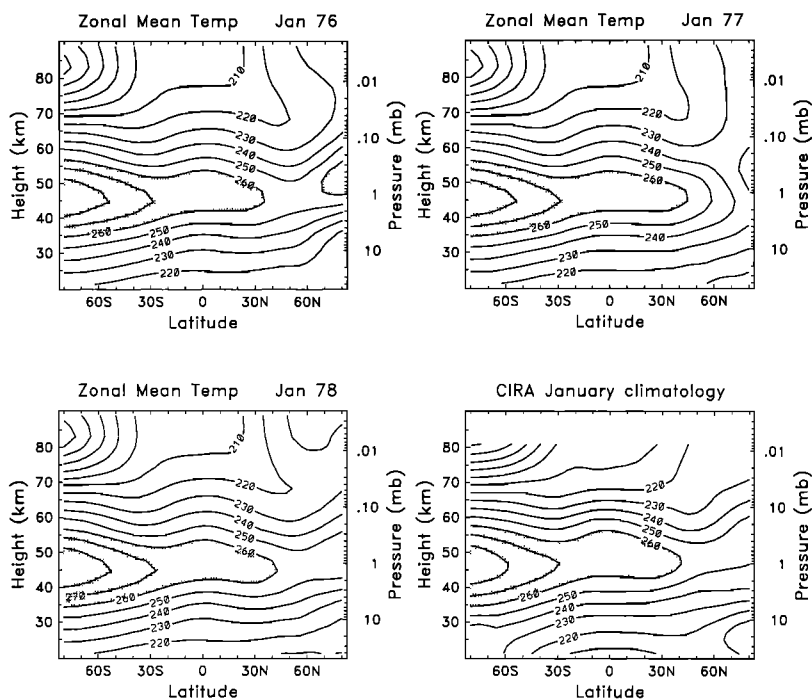


Figure 1. Zonal-mean monthly mean January temperature from the 3 pressure modulator radiometer (PMR) years and the *Barnett and Corney* [1985] climatology.

matology is less sensitive to vertical gradients than the reretrieved PMR data. This conclusion is supported by comparisons between CIRA86 and other climatologies [e.g., *Clancy and Rusch*, 1989; *Clancy et al.*, 1994] and must be due to either the poorer temperature retrievals used originally or the inadequacies in the merging and averaging procedure used to create the CIRA86 climatology.

2.2. The Separated Stratopause

The presence of a warm stratopause in the polar night is of interest since it must be of dynamical origin (in the polar night, there can be no solar heating to produce a stratopause). The separated stratopause was first described by *Kanzawa* [1989] using CIRA climatological data and examined more closely by *Hitchman*

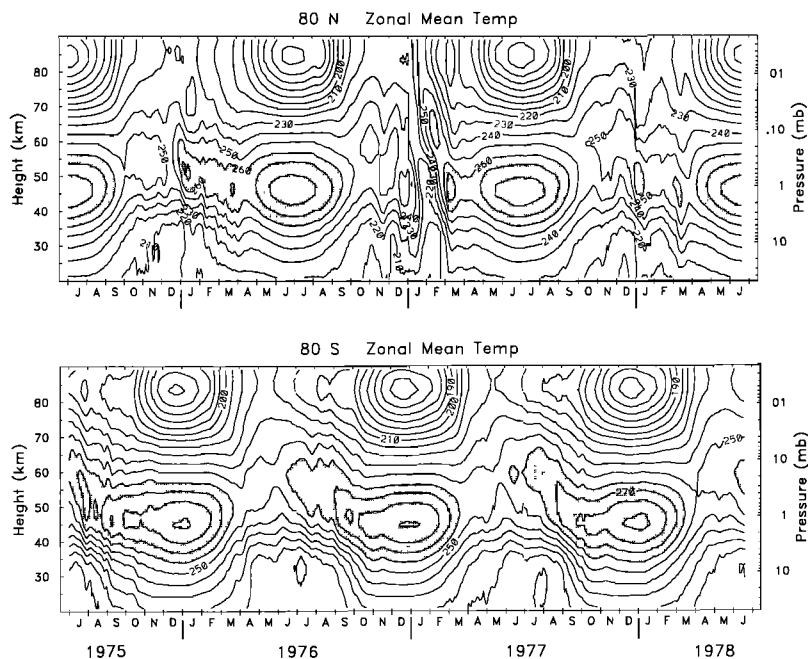


Figure 2. Zonal-mean temperature at 80°N (upper panel) and 80°S (lower panel) for the duration of the PMR data collection.

et al. [1989], who point out the salient features. Both papers state that it is a much stronger feature in the southern hemisphere. However, examination of the individual years leads one to conclude that on occasion it can be a very pronounced feature in the northern hemisphere as well.

If we compare the January means for the three individual years (Figure 1), we can see that there is a significant amount of variability: January 1976 shows a polar stratopause at least 10 K warmer than midlatitudes, and January 1978 shows a weaker but similar polar maximum. January 1977 is very different from these other years, exhibiting polar temperatures much colder than midlatitudes and a weak, low stratopause. For the corresponding months in the southern hemisphere, the separated stratopause is very prominent each year. The CIRA86 climatology shows a somewhat stronger feature, probably due to the fact that the separated stratopause occurs precisely where the SCR and PMR data sets are merged in the climatology (it should be recalled that the SCR data are from different years).

Figure 2 shows altitude-time sections of the temperatures at 80°N and 80°S illustrating evolution of the polar stratopause. A repeatable annual cycle is seen in the southern hemisphere (SH), whereas the NH ex-

hibits intense winter variations. It can be seen that in February 1977, the region of elevated temperatures in the NH was much higher and stronger than the other years. In the climatology, it can be seen that the averaging process has highlighted the southern separated stratopause due to the interannual repeatability, in contrast with the north, where the averaging of the interannual variability has hidden the occasionally intense feature.

2.3. The Zonal-Mean Zonal Wind

We begin by showing the seasonal evolution of the zonal wind at 1, 0.1, and 0.01 hPa as a function of latitude (Figure 3). At 1 hPa, the contrast between the three different northern hemisphere winters is apparent; each year has different timing and position of winter jet maxima, which is evidence of quite different winter vortex structure. The relatively regular seasonal march in the southern hemisphere is also clear. A comparison from one year to the next of the distance of penetration of the southern hemisphere summer easterlies into the northern hemisphere seems to imply high repeatability. At 0.1 hPa and above, the difference between the northern winters is even more apparent, with markedly different jet structures from one year to the next. In the

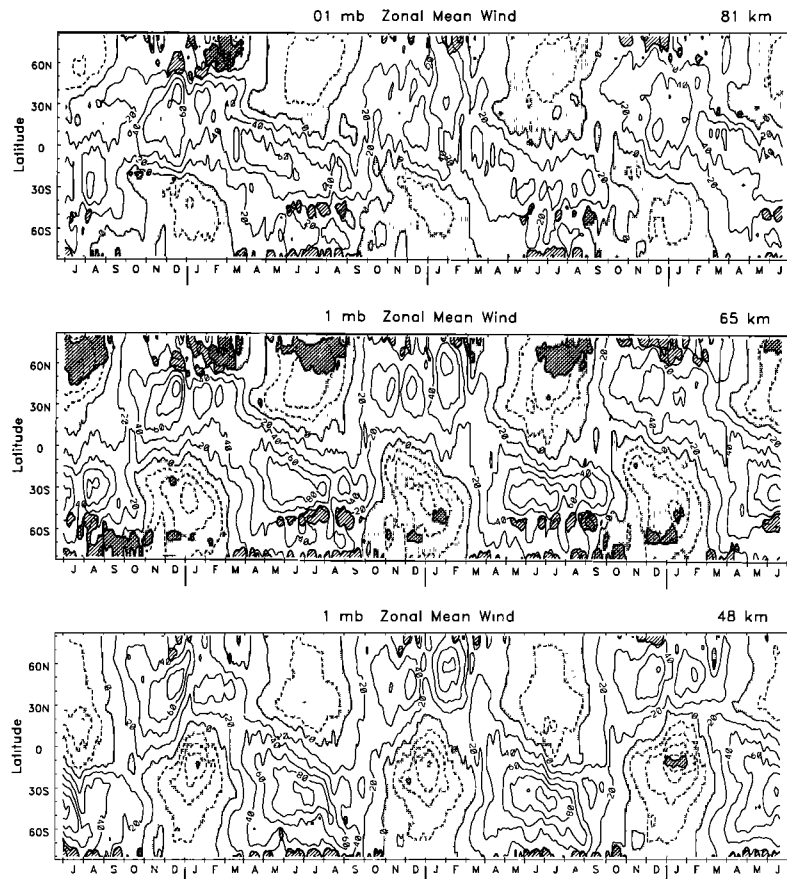


Figure 3. Zonal-mean zonal wind over the PMR period at (top to bottom) 0.01, 0.1, and 1 hPa. Easterlies are lightly shaded, and the dark shading denotes regions where the gradient of quasi-geostrophic potential vorticity is strongly negative (see text).

south, the mesospheric wind regime is not so repeatable between years as it is in the stratosphere. Although the balance assumption used to derive the wind at 80 km is probably quite poor in the tropics, one can see that in the extratropics the mean flow is characterized by much smaller scales and more rapid variation. There is clearly considerably more interannual variability than lower down, although the strength of the circulation as indicated by the jet maxima is fairly consistent in the summer regions.

Figure 3 also includes heavy shading indicating regions where the quasi-geostrophic potential vorticity gradient (\bar{q}_y) is significantly negative ($\bar{q}_y \leq -1.5 \times 10^{-11} \text{ m}^{-1} \text{ s}^{-1}$), potentially indicative of dynamic instability of the zonal-mean flow [Andrews *et al.*, 1987]. Regions of persistent negative \bar{q}_y are found in the SH winter mesosphere on the poleward side of the subtropical jet (near 50°S) and also at high latitudes throughout the stratosphere and mesosphere. These regions are associated with the appearance of the 4-day wave over polar latitudes in SH winter, as discussed in more detail below. A second region of persistent negative \bar{q}_y is found in the summer mesosphere at high altitudes (near 65 km) on the poleward side of the easterly jet, particularly in the NH. Pfister [1985] and Elson [1990] have analyzed instabilities of jet structures similar to those found in this region, finding strong growth rates. Nonetheless, we do not find evidence of transient waves in the summer mesosphere in the PMR data, possibly because of the low vertical resolution.

Latitude-height sections of the zonal-mean zonal wind

in January of each year of the Nimbus 6 period are displayed in Figure 4. For comparison, the winds derived from CIRA86 using the same computational domain and scheme are also displayed. The major features in January are the summer mesospheric jet, the subtropical summer stratospheric jet, the winter mesospheric jet, and the stratospheric polar night jet. The evolution of these features is well characterized in the previous time series. These figures allow one to conclude that the main structures are relatively repeatable from one year to the next, but the strength and position of both the winter mesospheric jet and the stratospheric polar night jet vary according to the dynamics of the winter in question (in particular, due to the timing and strength of any stratospheric warmings). The situation in the southern winter August is similar to that of the northern January, as can be seen in Figure 5, which displays sections for the three Augusts (and that of the CIRA86 climatology). It is apparent from these sections that the summer mesospheric jet is much weaker in the NH than in the SH and also that the SH subtropical mesospheric westerly jet is more narrow and intense than the NH counterpart. There is less interannual variability in the SH stratospheric polar night jet than in the NH, so that the climatology is closer to individual years. However, the patch of easterlies in August 1975 at high southern latitudes and high altitudes is a salutary reminder that there is still considerable variability in the SH (see also Figure 6). One can also see that the CIRA86 climatology (which in the mesosphere is solely due to an average of the 3 years of the PMR data), has

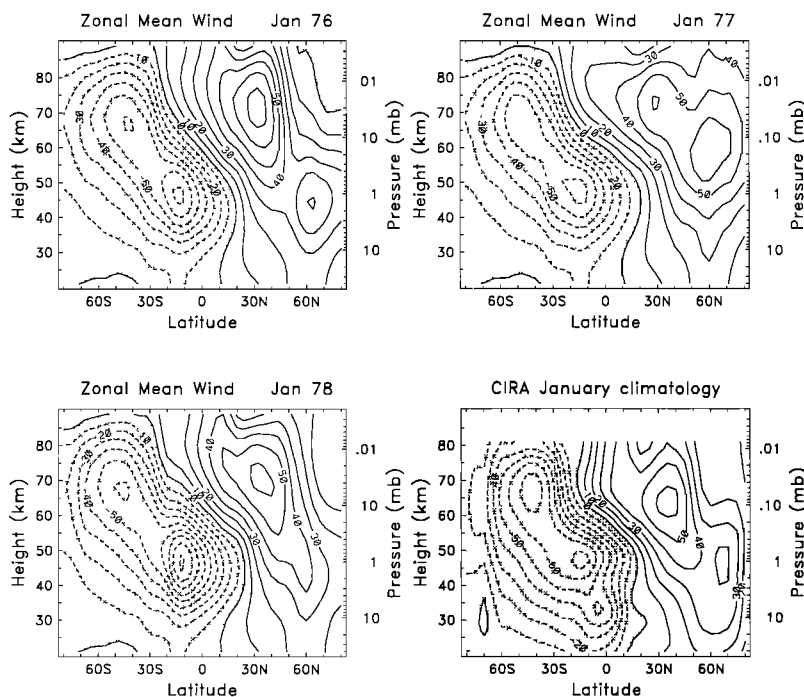


Figure 4. Zonal-mean monthly mean January zonal wind from the 3 PMR years and the Barnett and Corney [1985] climatology.

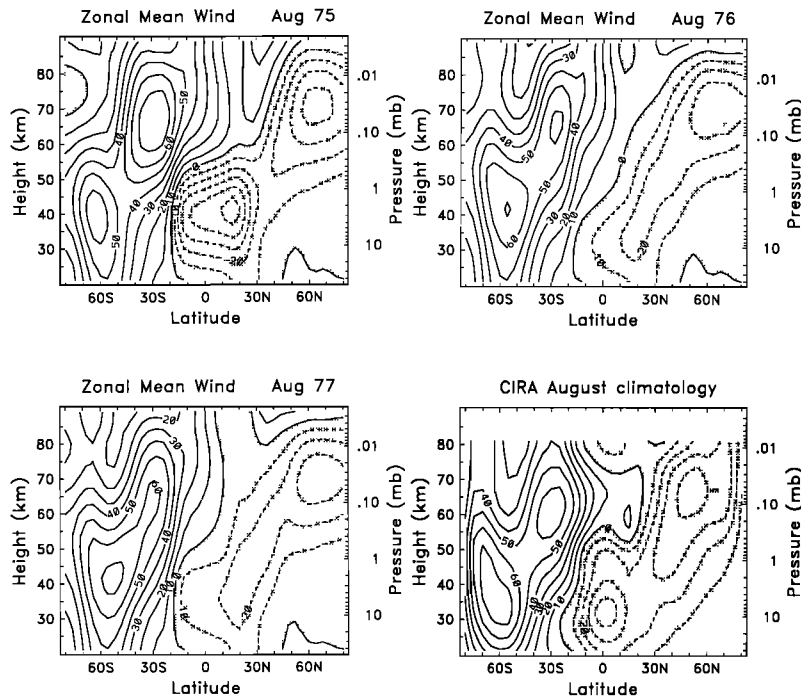


Figure 5. Zonal-mean monthly-mean August zonal wind from the three PMR years and the Barnett and Corney [1985] climatology.

introduced spurious structures in the mesosphere (such as the westerly jet peak found at about 20°N and 60 km). Such artifacts can also be found in other months.

3. Daily Variability

Previous workers have looked at the planetary wave structure in the mesosphere observed by the PMR instrument by concentrating on the raw radiance data

[e.g., Labitzke and Barnett, 1981; Hirota and Barnett, 1977; Hass and Ebel, 1986]. Here we concentrate on the variability occurring on faster than seasonal timescales in temperature, wind, and derived quantities associated with planetary waves.

The broad scope of variability over the period is well characterized by the root-mean-square deviation from the zonal-mean, and for an overview, we display this for the geopotential height of two pressure levels, 3 hPa

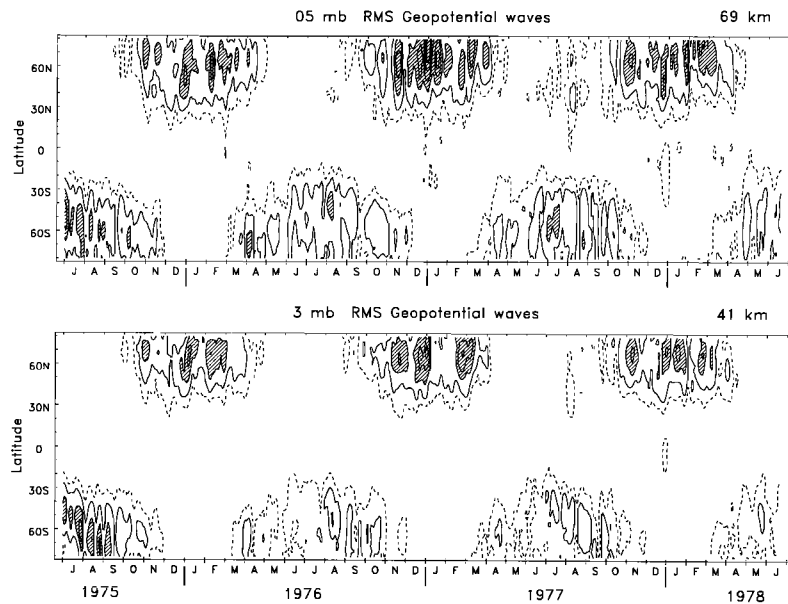


Figure 6. Latitude-time sections of the rms geopotential height around the zonal-mean at 3 hPa (~ 41 km) and 0.05 hPa (~ 69 km). Contour interval (solid lines) is 300 m, with values above 600 m hatched. The dashed line is the 150-m contour.

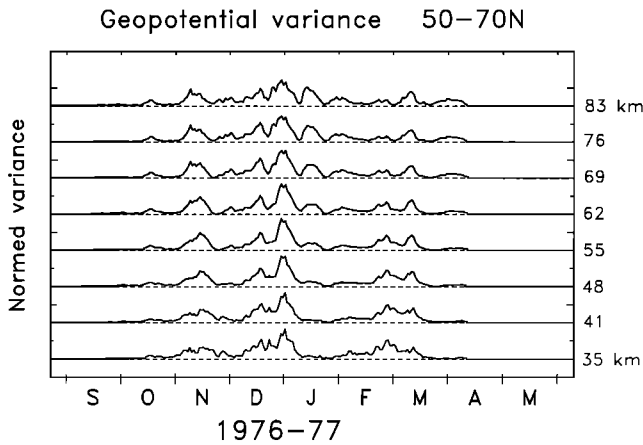


Figure 7. Time variation of rms geopotential height amplitude over 50°-70°N at eight altitude levels (separated by approximately one scale height) during northern hemisphere winter 1976-1977. Amplitudes at each level have been normalized to unit variance.

(~41 km) and 0.05 hPa (~69 km), representative of the upper stratosphere and middle mesosphere in Figure 6.

Much of the variability in the mesosphere is of stratospheric origin, and we begin below by assessing the importance of direct dynamic coupling between the stratosphere and the mesosphere. In addition, a significant contribution to mesospheric variability comes from within: Two well-known examples (the 4-day wave and normal mode oscillations) are examined in detail below. However, much of the variability seen in Figure 6 is probably ultimately due to the affect of breaking gravity waves [e.g., *Smith, 1996*] which we cannot examine here.

3.1. Stratosphere-Mesosphere Coupling

As seen in Figure 6 large-amplitude, episodic wave-like events are observed in each winter hemisphere, with typically three to six individual events, or "pulses," seen

each season. Such wave growth events are well correlated with the zonal wind decelerations over 30-65 km seen in Figure 3 (this correlation is less evident for the 0.01 hPa winds in Figure 3). At first inspection, many of the individual pulses in Figure 6 are approximately correlated between the 41 and 69 km levels, although the detailed evolution is clearly different at each altitude. To examine vertical correlation in more detail, Figure 7 shows time variation of geopotential wave variance near 60°N during NH winter 1976-1977, at eight altitude levels spanning 35-83 km (each level is approximately one scale height, 7 km, apart). For most of the events in Figure 7, wave variance maxima are observed at all levels throughout the stratosphere and mesosphere, demonstrating that these transient events span the entire middle atmosphere (~30-90 km). One notable exception is the wave event near the middle of January in Figure 7, which reaches large amplitude in the mesosphere (above 50 km) but not in the stratosphere.

The spatial patterns of the zonal-mean temperature and wind changes during these events show strong coupling between the stratosphere and mesosphere, as is expected during periods of massive polar vortex disruption. Figure 8 shows the temperature and wind changes associated with the beginning of the major warming during late December 1976. The temperature change between the December 24, 1976, and January 1, 1977, exhibits a clean quadrupole pattern, with high-latitude warming and tropical cooling in the stratosphere and reversed patterns in the mesosphere. Such temperature patterns have been shown previously [e.g., *Fritz and Soules, 1970; Labitzke, 1972; Gille et al., 1983*] and are in good agreement with theoretical expectations for winter hemisphere planetary wave events [*Garcia, 1987*].

The zonal wind changes in Figure 8 show deceleration of the winter hemisphere jet from the middle stratosphere to the middle mesosphere (over 30-70 km, in accord with the subjective impression described above) and easterly accelerations in the tropics (in balance with

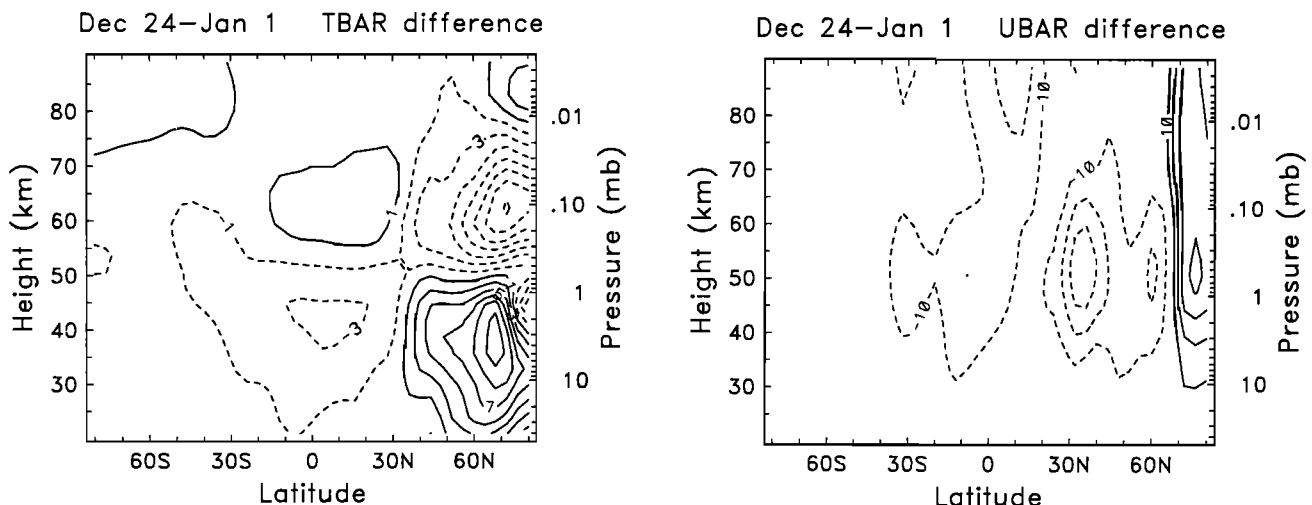


Figure 8. Changes in the zonal-mean state between December 24, 1976, and January 1, 1977: zonal-mean temperature differences (left panel) and zonal-mean wind differences (right panel).

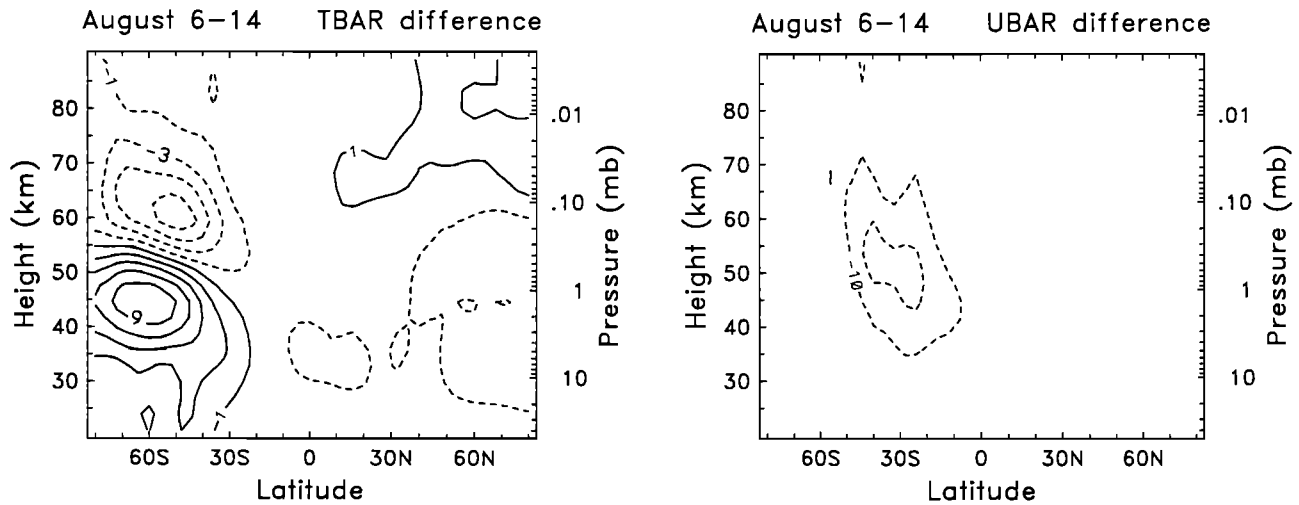


Figure 9. Changes in the zonal-mean state between August 6 and 14, 1976: zonal-mean temperature differences (left panel) and zonal-mean wind differences (right panel).

the tropical temperature changes). Figure 9 shows similar diagrams for a wave event during SH winter (August 6-15, 1976). The patterns of temperature and wind changes are similar to the NH example (Figure 8), but are somewhat weaker in amplitude (consistent with the weaker-amplitude planetary waves observed in the SH; see below). (Examination of time series and other years of data shows that the NH high-latitude temperature changes in Figure 9 are related to the seasonal cycle rather than to planetary-wave-induced transience.)

In the NH upper stratosphere, large-amplitude wave transience is usually associated with massive disturbances of the polar vortex as anticyclonic vortices form in the upper stratosphere which are associated with stratospheric warmings of various strengths. Analysis of the pulses seen in Figure 7 shows that each of them is associated with strong vortex disturbances and consequently most of the variance is concentrated in zonal wave numbers 1 and 2. The large pulse at the end of December is associated with the beginning of the major midwinter warming and the destruction of the lower stratospheric vortex described by *Labitzke and Barnett* [1981] and *Labitzke et al.* [1993]. During the period while there was no lower stratospheric polar vortex, the mesosphere still maintained a strong vortex, probably due to the strong radiative cooling there. Following this period, it appears that air brought poleward became associated with a mesospheric high (similar to Figure 17 of *Dunkerton and Delisi* [1985]). This latter episode, which didn't involve simple wave propagation from below, resulted in the pulse-like event seen only in the mesosphere in Figure 7.

3.2. Normal Modes

Normal-mode Rossby waves are westward propagating planetary waves which are the free or resonant oscillations of the atmosphere. Their basic characteristics

are governed by the resonant properties of the atmosphere, rather than by the details of any forcing mechanisms. The fundamental signatures of these modes are planetary-scale horizontal structures, regular westward propagation at (nearly) discrete frequencies with typical periods of 5-20 days, and small vertical phase tilts with height (see the review by *Madden* [1979]). Numerous studies have identified normal-mode structures in stratospheric data derived from satellite measurements [e.g., *Rodgers*, 1976; *Hirota and Hirooka*, 1984; *Hirooka and Hirota*, 1985, 1989; *Prata*, 1989; *Venne*, 1989; *Randel*, 1993a]. Typically, identification as normal modes in these studies is based both on enhanced spectral power

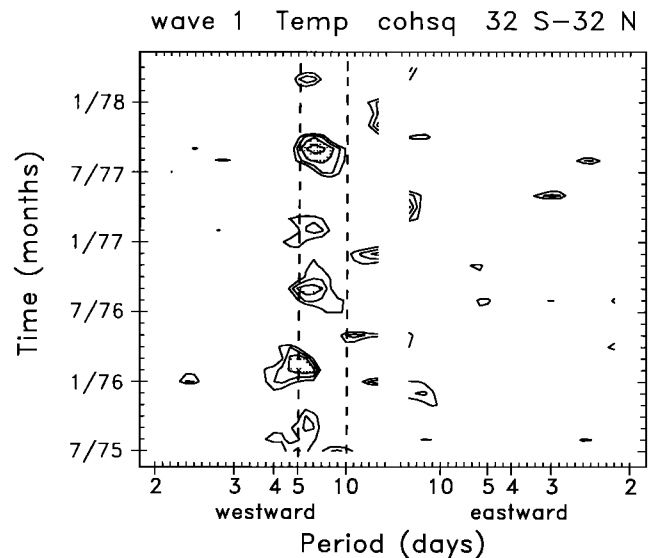


Figure 10. Coherence squared spectra between 32°N and 32°S for zonal wave 1 temperature fluctuations at 0.1 hPa (~ 65 km) throughout the PMR record. Spectra are calculated from overlapping 60-day time series. Note the coherence maxima for 5- to 10-day westward traveling waves near March and October of each year.

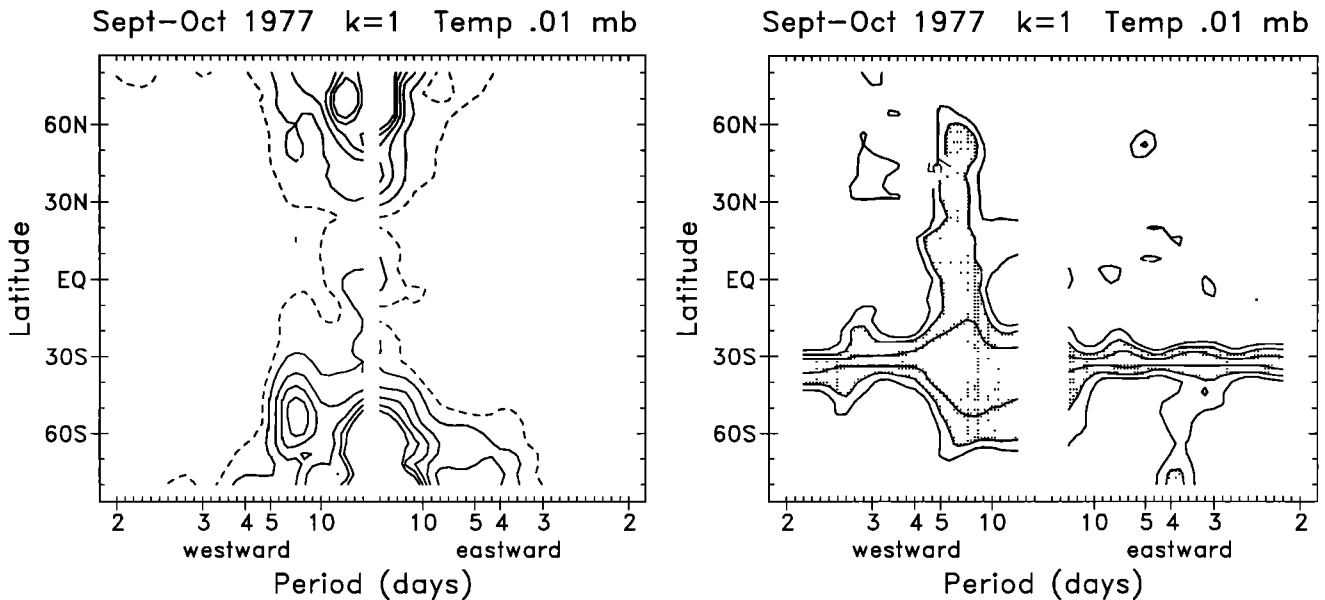


Figure 11. Latitude-frequency spectra for zonal wave 1 temperature fluctuations at 0.01 hPa (~ 81 km) during October 1977. Left panel shows power spectra (contours are arbitrary; dashed line is one half lowest level), and right panel shows coherence squared at each latitude with respect to 32°S .

and global coherence for westward propagating planetary waves near the appropriate normal-mode frequencies and on horizontal and vertical structures consistent with theoretical predictions (calculated structures are given by *Kasahara* [1980], *Schoeberl and Clark* [1980], and *Salby* [1981]). We follow this method by searching for normal-mode signatures in power and coherence spectra and then examining the spatial structure of the modes during periods of large wave amplitude. Our focus is on mesospheric waves and zonal wave number 1 features (higher wave numbers do not exhibit clear evidence as that seen for wave 1, possibly due to the vertical resolution).

The occurrence of global normal modes in the mesosphere throughout the PMR record is investigated in Figure 10, which shows the coherence squared between 32°N and 32°S for zonal wave 1 temperature at 0.1 hPa, constructed from overlapping 60-day spectra throughout the record. Figure 10 shows occurrence of coherent global westward propagating waves near each March and October (equinox seasons), with periods in the 5- to 10-day range. The appearance each March and October of the coherence maxima in Figure 10 is quite striking, showing that such modes are a regular feature of the mesosphere.

Two individual periods are shown in more detail: October 1977 at 0.01 hPa (Figure 11) and March-April 1976 at 0.1 hPa (Figure 12). Both power spectra and coherence squared are shown for temperature fluctuations and geopotential fluctuations, respectively. Clear spectral peaks are visible in both hemispheres for both cases; both the 5- to 10-day periodicity in October and the 5-day periodicity in March-April show near global

coherence. The combination of enhanced power and near-global coherence for discrete (westward) frequency bands is strong evidence of normal-mode oscillations. The spectral power density for these waves is generally a small fraction of the total (i.e., the waves are usually of small amplitude, although periods of large amplitude do occur). The global coherence (seen in Figures 11 and 12) is often a more sensitive diagnostic for the presence of normal modes than the occurrence of peaks in power spectra alone.

The structure of the dominant mode during September-October 1977 (the time period of Fig 11) is shown in more detail in Figure 13. Here the amplitude and phase of the westward 5- to 10-day-period waves seen in geopotential height amplitude and phase are displayed (we have resynthesised time series from windowed spectral coefficients and then averaged in time over several weeks of large wave amplitude). The amplitude exhibits broad maxima over midlatitudes of both hemispheres, with nearly in-phase (symmetric) horizontal structure between the NH and SH and weak westward phase tilts with height. Figure 13 also shows the temperature structure for this spectral band, showing in-phase latitudinal structure and vertically out-of-phase temperature maxima near the stratopause (~ 50 km) and in the middle-upper mesosphere. The in-phase latitudinal structure seen in Figure 13 is a characteristic observed of each of the equinox coherence maxima identified in Figure 10. The amplitude peaks are roughly colocated with the background zonal jet maxima, as can be seen in Fig 14, where we have superimposed the geopotential maxima from Figure 13 as bold lines upon the zonal wind fields. The slight NH-SH asymmetry is mirrored in

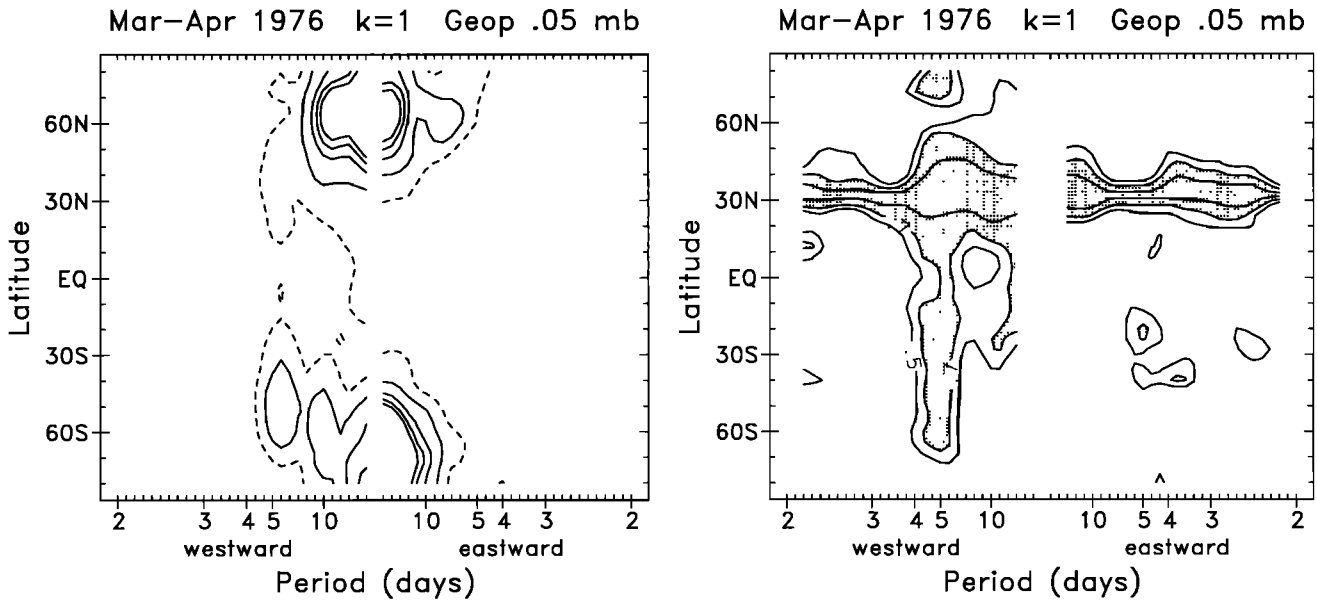


Figure 12. Latitude-frequency sections of power and coherence squared (with respect to 32°N) for zonal wave 1 geopotential fluctuations at 0.05 hPa (~ 69 km) during March-April 1976.

both the zonal wind and wave amplitude structure. It is likely that occurrence of similar symmetric background winds is associated with the presence of normal-mode oscillations each equinox season (seen in Figure 10).

3.3. 4-Day Wave

A zonal wave number 1 feature, with a period near 4 days, was first observed in SCR temperature data by *Venne and Stanford* [1979]. Further analysis by those authors and others has shown that the wave is almost an ubiquitous feature of the winter polar stratosphere and that it occurs in the winter of both hemispheres, although the signal is usually stronger in the south. *Prata* [1984] and *Lait and Stanford* [1988] showed that the wave is associated with higher zonal wave number disturbances which are phase-locked to the wave 1 component. They also showed that the resultant wave structure is associated with warm pools of air rotating around the polar vortex. The vertical extent of these waves was demonstrated by *Lawrence et al.* [1995], who showed evidence for their penetration up to 90 km by examining radar wind data from Scott Base (79°S). Theoretical analyses of the mean flow in the winter polar middle atmosphere [*Hartmann, 1983; Randel and Lait, 1991; Manney and Randel, 1993*] along with observations [*Manney, 1991*] have demonstrated that instability mechanisms in the upper stratosphere and mesosphere provide a plausible explanation for the development of the 4-day wave.

The 4-day wave has been observed in PMR data before [*Prata, 1984*]; here we concentrate on the structure and variability of the 4-day wave observed in the PMR data. We begin by using space-time spectral analysis to demonstrate the occurrence and strength of the 4-

day wave. Power spectra over polar latitudes are constructed from overlapping 60-day time series and plotted versus time (Figure 15). In addition to the low-frequency maxima in the respective winter seasons and near-zero wave variance in summer, the 72°S spectra show spectral maxima corresponding to an eastward traveling wave with a period near 4 days during SH mid-winter in 1976 and 1977 (early SH winter 1977 also exhibits eastward propagating variance at slightly longer periods of 5-10 days). The NH spectra in Figure 15 do not exhibit similar strong peaks near the 4-day period, although weak 4- to 5-day maxima are observed near November of each year.

The structure of the wave is demonstrated by highlighting the SH event of August-September 1977. Figure 16 shows meridional cross sections of variables characterizing the event averaged over September 1-7, 1977. The 4-day wave signature is extracted from the data by resynthesis of the space-time harmonic coefficients, retaining only components corresponding to eastward traveling waves with periods near 4 days. Eddy wind coefficients are then calculated using balance wind assumptions, and the Eliassen-Palm (EP) flux divergence is calculated neglecting the vertical velocity term. The EP flux divergence shows a north-south dipole pattern which is mostly attributable to the horizontal EP flux component (proportional to the momentum flux, which is equatorward).

Figure 16 also shows the zonal wind for this time period, with shaded regions denoting negative quasi-geostrophic potential vorticity gradients ($\bar{q}_y < 0$). The zonal wind structure is dominated by a strong jet in the SH subtropical mesosphere, apparently decoupled from the upward extension of the high-latitude stratospheric

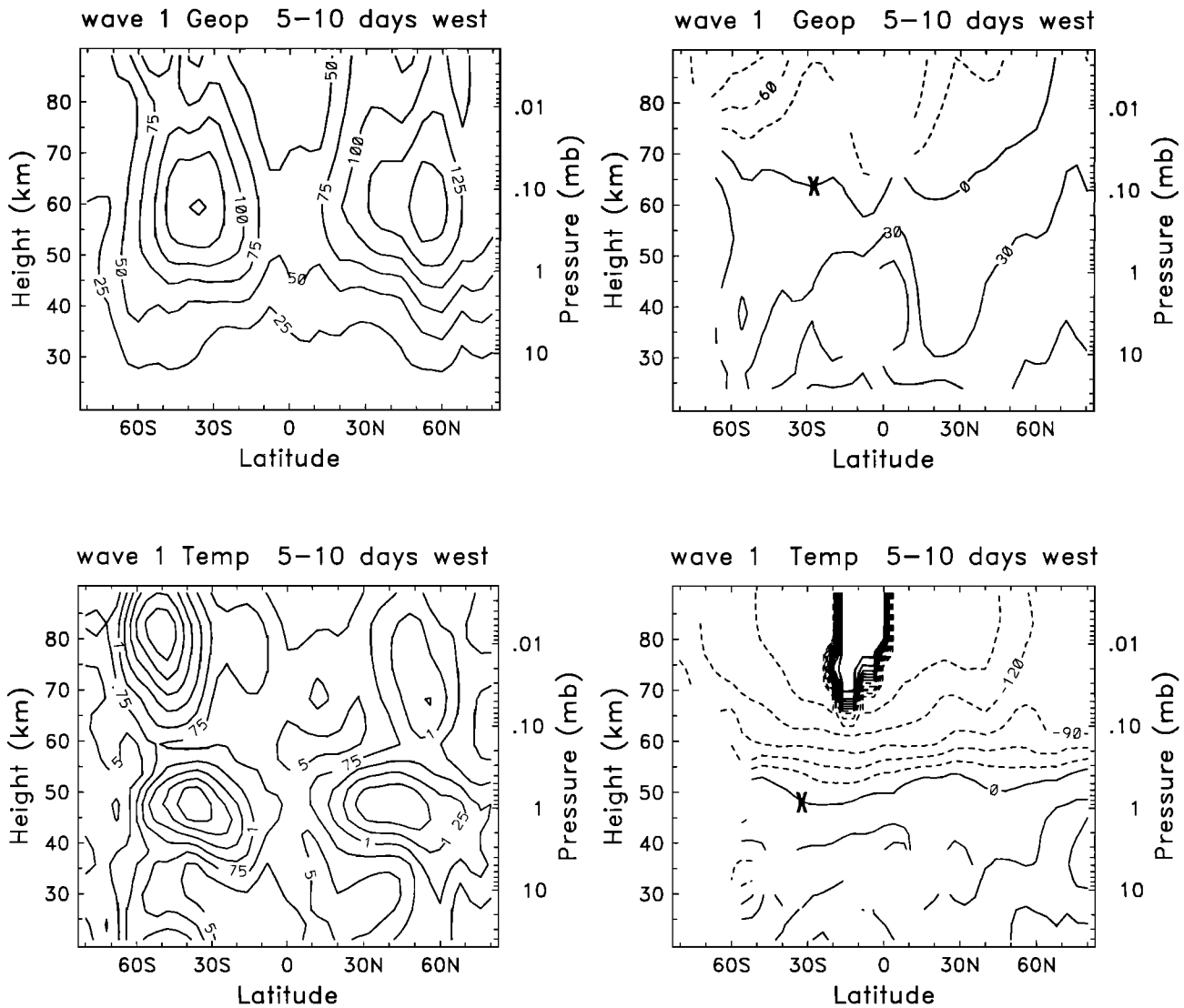


Figure 13. Meridional cross sections of geopotential (upper panels) and temperature (lower panels) amplitude and phase for westward traveling zonal wave 1 with 5- to 10-day periods during October 1977. The phases are calculated with respect to the mean altitude maxima as marked.

polar night jet (compare with the monthly averaged structure shown in Figure 5). The resulting “double jet” structure has marked curvature and strongly negative potential vorticity (PV) gradients over 45°–60°S throughout the mesosphere.

Figure 17 shows time series of 4-day wave geopotential amplitude and EP flux divergence at 60°S, 0.2 hPa during 1977. These time series show several episodes of wave growth and decay throughout the SH winter, with a large event in early September (the time period sampled in Figure 16). Also shown in Figure 17 is evolution of the 0.1-hPa zonal wind at 32°S and 56°S, together with the 0.1-hPa potential vorticity (PV) gradient at 56°S. The wave and mean flow time series in Figure 17 show clear temporal coupling: the wave growth events (as seen in the EP-flux divergence) are coincident with

negative \bar{q}_y , which are in turn related to opposing mean flow changes at 32°S and 56°S. The zonal winds at 56°S exhibit decelerations just prior to growth of the 4-day wave, while the jet near 32° intensifies. These changes strongly increase the horizontal wind shears (and curvature), resulting in the strongly negative PV gradient near 56°S occurring just prior to wave growth.

The temporal coincidence of wave growth with appearance of negative PV gradients (Figure 17) strongly suggests instability of the mesospheric jet structure as the cause of the 4-day wave. The source of the wave from instability is also suggested by the spatial coincidence of negative PV gradient and positive EP flux divergence seen in Figure 16 (near 50°–60°S, throughout the mesosphere). The spatial and temporal coincidence of these quantities can be a signature of an internal

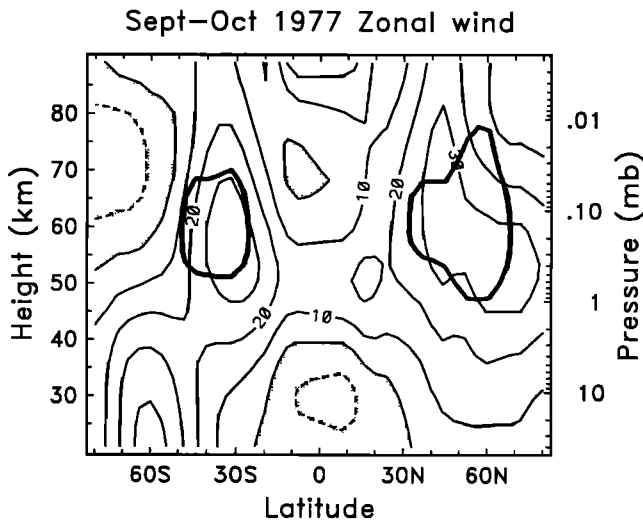


Figure 14. Zonal-mean zonal winds for October 1977. Bold lines denote geopotential maxima for the westward traveling wave isolated in Figure 13.

instability [see *Randel and Lait, 1991*]. The wave structure observed in Figure 16 (including the presence of downward pointing vectors near 60-65 km, which indicate a nonnegligible contribution from baroclinic wave processes) is also consistent with the instability calculations of *Manney and Randel [1993]*, performed for background zonal flows similar to that in Figure 16.

4. Discussion

The difficulties inherent in producing mesospheric climatologies, and in particular, comparing such climatologies from different periods and instruments are

well described by *Clancy et al. [1994]*. In their work, they describe differences of 5-20 K between the SME and the CIRA data in the lower mesosphere, with the SME being warmer. These results are consistent with ours (i.e., the newer PMR temperature retrievals being warmer) for some latitudes and years; however, differences of both signs were found, highlighting the difficulty of comparing data with different vertical resolutions. The additional problem for comparing climatologies from different periods is that they can time average data with high internal interannual variability; it is exemplified by the separated stratopause in the northern hemisphere and is highlighted here for the benefit of middle atmospheric modelers.

Much of the rapid transience seen in the zonal-mean fields (e.g., Figure 3) must be due to fluctuations in the gravity-wave driving, as conjectured by *Fritts and Vincent [1987]* among others. Here we show that there is also a significant component of fast zonal-mean variability resulting from large-scale transience in the stratosphere. The changes in zonal-mean temperature shown in Figures 8 and 9 are also consistent with changes in the residual mean circulation (e.g., Figure 8 of *Randel [1993b]*) and are evidence of global circulation cells which accompany winter hemisphere planetary wave events [*Garcia, 1987*].

In our analysis of the coupling of large-scale perturbations in the stratosphere to those in the mesosphere, interpretation in terms of wave propagation is complicated by the large vortex interactions high in the upper stratosphere where linear theory must break down. The well-known propensity of the polar vortex to suffer pulse-like distortions associated with sequences of warmings throughout winter [e.g., *Rosier et al., 1994*] is seen here. As has been found before [*Pierce et al.,*

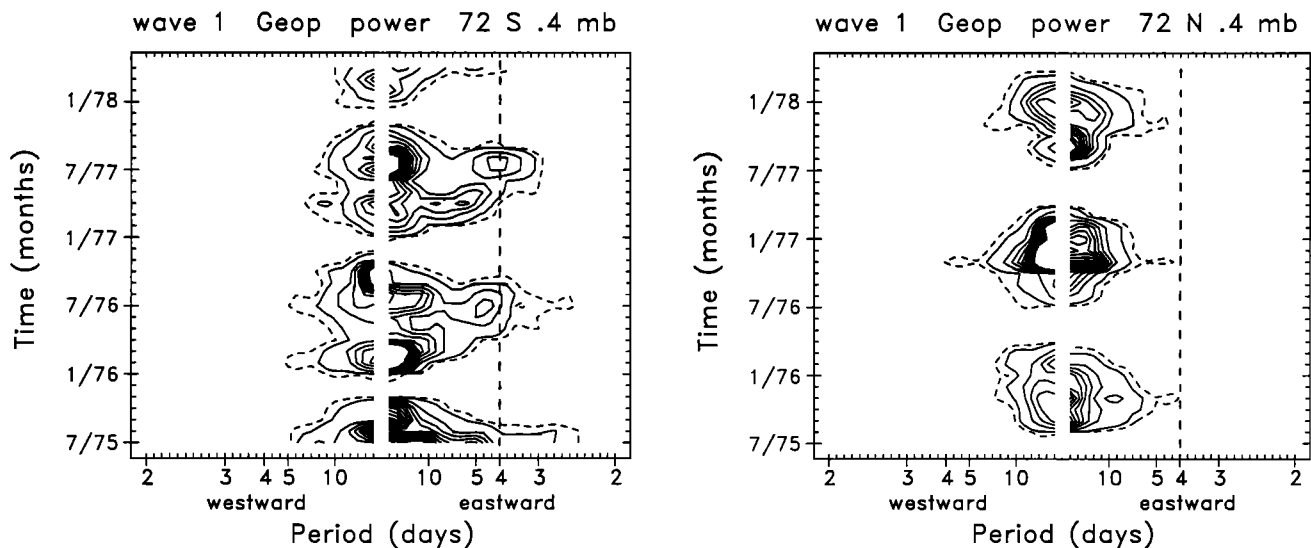


Figure 15. East-west power spectra for zonal wave 1 geopotential height fluctuations at 0.4 hPa (~ 55 km) for data at 72°S (left) and 72°N (right). Spectra are calculated from overlapping 60-day time series throughout the PMR record. Note the spectral peaks corresponding to eastward traveling waves with periods near 4 days during southern hemisphere winter.

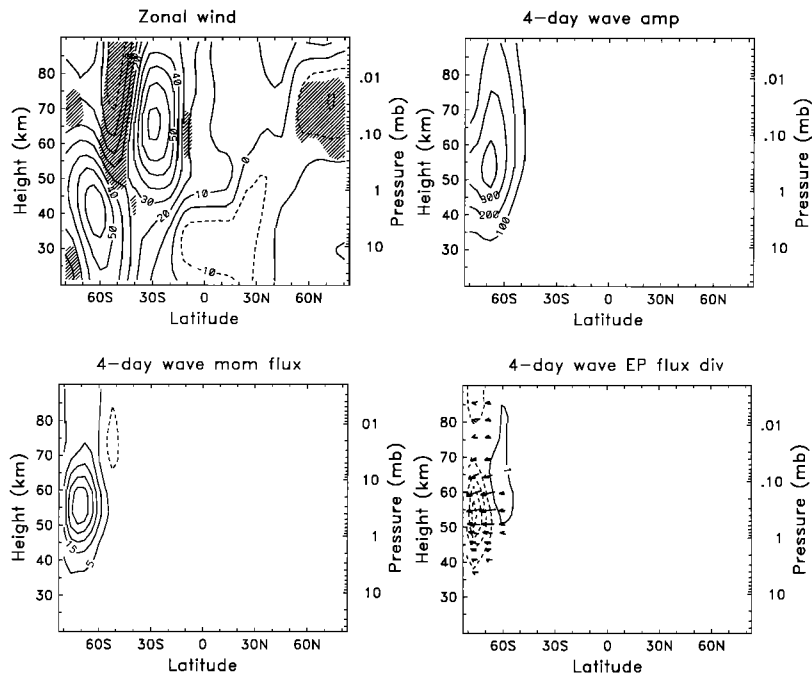


Figure 16. Meridional sections of zonal-mean wind (upper left) and 4-day wave geopotential height (upper right) and northward momentum flux (lower left) and Eliassen-Palm (EP) flux signature (lower right) during a large amplitude wave event in September 1977. Shading in the zonal wind denotes regions of negative potential vorticity gradient. Contours of the EP flux divergence are $\pm 1, 2, \dots, \text{m s}^{-1} \text{d}^{-1}$.

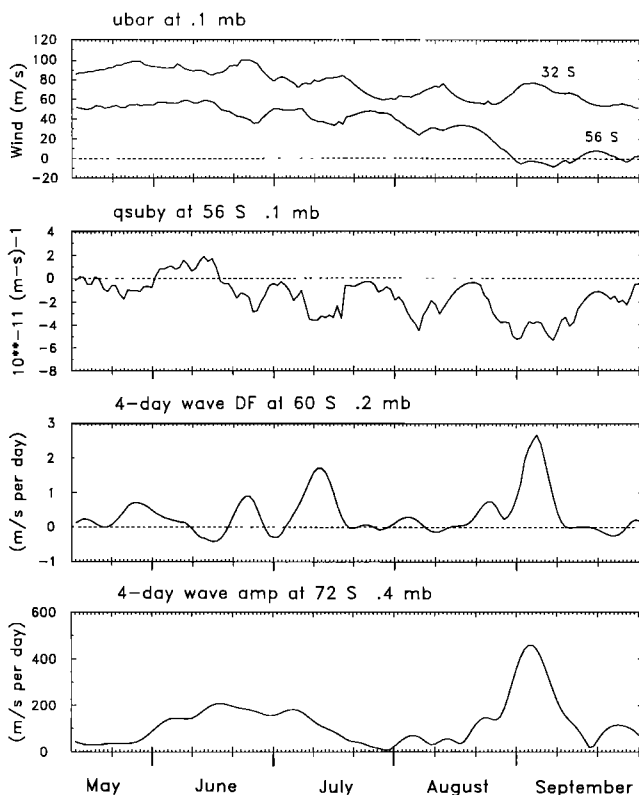


Figure 17. Time series of background mean flow and 4-day wave quantities during May-September 1977. Shown from top to bottom are the 0.1-hPa zonal wind at 32°S and 56°S; quasi-geostrophic potential gradient at 56°S, 0.1 hPa; EP flux divergence at 60°S, 0.2 hPa; and geopotential height amplitude at 72°S, 0.4 hPa.

1993], such pulses are not always obviously associated with pulses from the troposphere and cannot easily be interpreted as Rossby-wave events.

The actual mesosphere is even more disturbed than the PMR observations suggest. Both rocket data [e.g., *Leovy and Ackerman, 1973*] and satellite data (*Miles and Grose [1989]* and the more recent high-resolution temperature retrievals provided by ISAMS) show phenomena with periods of a day to a few days and small vertical scales which would not be visible in the PMR data. Indeed, *Leovy and Ackerman [1973]* state in their analysis of rocket data that the main feature of interest is the change from remarkable steady flow below 45 km to strongly oscillating flow above 50 km, and this is consistent with the more recent satellite data (including direct wind observations from the high resolution Doppler interferometer aboard UARS). The PMR data don't show such an obvious change, which again is probably due to the poor vertical resolution of the retrievals.

Such small-scale phenomena are probably due to a number of causes: Obviously, fluctuations in the source strength and propagation conditions will lead to variability in gravity wave driving. The further influence of nonlinearity [e.g., *Dunkerton and Delisi, 1985*] upon upward propagating disturbances (such as those described above) and both local barotropic and baroclinic instability must also contribute. This latter prospect is consistent with our calculations that the meridional gradient of zonal-mean potential vorticity often changes sign on the poleward flank of the mesospheric jet, and toward the pole, during winter (thus satisfying the nec-

essary conditions for mean flows to be unstable). Since the zonal-mean flow itself exists in the presence of perturbations, it is highly likely that a local criterion for instability is satisfied throughout the polar winter mesosphere (Pedlosky [1979] presents an argument that simple instability analyses are probably biased toward stability). Further, given that the static stability in the mesosphere is as small as and often locally smaller than that in the troposphere, disturbances with horizontal scales of the order of 1-2000 km might be expected. However, unlike the troposphere, disturbances in the mesosphere are subject to rapid radiative and dynamical damping, so many such disturbances may not develop into planetary-scale waves, even when they might be locally large for short periods of time. The manifestation of these sort of phenomena in the PMR data may well be the small anticyclones that can be seen persisting for short periods of time in synoptic maps of geopotential height in the mesosphere.

Although the PMR data don't often directly show such small-scale phenomena, the effect of these scales is manifest in the calculations of Hass and Ebel [1986], who in an attempt to assess the efficiency of transport due to waves carried out an analysis of the integral scales present in the data. They found considerable spatial and temporal variability and, in particular, found timescales less than 5 days nearly everywhere in the upper mesosphere. This, coupled with their observation that if radiative processes were dominating then spatial fields should have been smoother than observed, leads one to conclude that the effect of the small scales can be found in the data even if it is not directly observed.

The major wave phenomena which are directly observable in the PMR data are the 4-day wave and the normal modes discussed above. The 4-day wave in the PMR data is prevalent throughout the southern winters observed, consistent with the repeated occurrence of negative gradients of potential vorticity that are observed in the winter mesosphere. Although the change in sign of \bar{q}_y is not a sufficient condition to indicate instability mechanisms, the coincidence of the negative PV gradients and positive EP flux divergences reported above are further indicators of internal instabilities. The lack of an obvious 4-day wave in the NH is consistent with the less negative \bar{q}_y and is probably due to the fact that the typical NH winter is characterized by massive transience in the background structure, associated with the series of minor and/or major warmings.

The power and coherence spectra calculated from PMR data show evidence of normal modes with periods in the (broad) 5- to 10-day band, all with symmetric latitudinal structure. The modes observed here with periods near 5 days appear to be manifestations of the first symmetric mode (often termed the "5-day wave," first analyzed in PMR radiance data by Prata [1989]). The most comprehensive numerical study of normal mode structures in realistic background flows is

that of Salby [1981]. His results show symmetric waves with periods near 5 days and in the range of 11-20 days, while the first antisymmetric mode (latitudinally out of phase between hemispheres) has periods of 8-11 days. The 5- to 10-day modes seen in the PMR data appear very similar overall to the calculated symmetric 5-day mode, although Salby's results suggest little spread of enhanced response beyond periods of 4.4-5.7 days, in contrast to the lower frequencies seen in the PMR data.

Acknowledgments. This work is based on the considerable effort of Clive Rodgers, John Barnett, and the original PMR team with the PMR instrument. We are indebted to Clive for providing the new PMR temperature retrievals and to John for providing the CIRA86 data in numerical form. Both Clive and John have been invaluable sources of information about the data. We are also grateful to John Gille and Dan Packman for taking the along-track data and converting it into a global grid. B.N.L. acknowledges the support of the Natural Environment Research Council, the inspiration of Sean Fitzpatrick and his team, and a number of useful conversations with David Andrews and Alan O'Neill. W.J.R. acknowledges support from NASA grants W-16215 and W-18181.

References

- Andrews, D. G., J. R. Holton, and C. B. Leovy, *Middle Atmosphere Dynamics*. Academic Press, Inc., San Diego, Calif., 1987.
- Barnett, J., and M. Corney, Middle atmosphere reference model derived from satellite data, in *Atmospheric Structure and Its Variation in the Region 20 to 120 km*, edited by K. Labitzke, J. Barnett, and B. Edwards, vol. 16 of *Handbook for MAP*, pp. 47-85. Univ. of Ill., Urbana, 1985.
- Clancy, R., and D. W. Rusch, Climatology and trends of mesospheric (58-90 km) temperatures based upon 1982-1986 SME limb scattering profiles, *J. Geophys. Res.*, *94*, 3377-3393, 1989.
- Clancy, R. T., D. W. Rusch, and M. T. Callan, Temperature minima in the average thermal structure of the middle mesosphere (70-80 km) from analysis of 40- to 92-km SME global temperature profiles, *J. Geophys. Res.*, *99*, 19,001-19,020, 1994.
- Curtis, P., J. Houghton, G. Peskett, and C. Rodgers, Remote sounding of atmospheric temperature from satellites V. The pressure modulator radiometer for Nimbus F, *Proc. R. Soc. London A*, *397*, 135-150, 1973.
- Dunkerton, T. J., and D. P. Delisi, The subtropical mesospheric jet observed by the Nimbus 7 limb infrared monitor of the stratosphere, *J. Geophys. Res.*, *90*, 10,681-10,692, 1985.
- Elson, L. S., Satellite observations of instability in the middle atmosphere, *J. Atmos. Sci.*, *47*, 1065-1074, 1990.
- Fleming, E. L., S. Chandra, J. Barnett, and M. Corney, Zonal mean temperature, pressure, zonal wind and geopotential height as functions of latitude, *Adv. Space Res.*, *10*, 1211-1259, 1990.
- Fritts, D. C., and R. A. Vincent, Mesospheric momentum flux studies at Adelaide, Australia: Observations and a gravity wave-tidal interaction model, *J. Atmos. Sci.*, *44*, 605-619, 1987.
- Fritz, S., and S. Soules, Large-scale temperature changes in the stratosphere, *J. Atmos. Sci.*, *27*, 1091-1097, 1970.
- Garcia, R. R., On the mean meridional circulation of the middle atmosphere, *J. Atmos. Sci.*, *44*, 3599-3609, 1987.

- Gille, J. G., P. L. Bailey, L. V. Lyjak, and J. M. Russel III, Results from the LIMS experiment for the PMP-1 winter 1978/79, *Adv. Space Res.*, **2**, 163–167, 1983.
- Hartmann, D. L., Barotropic instability of the polar night jet stream, *J. Atmos. Sci.*, **40**, 817–835, 1983.
- Hass, H., and A. Ebel, Space and time scales of large scale variations in the upper stratosphere and mesosphere as deduced from the PMR of Nimbus 6, *J. Atmos. Terr. Phys.*, **48**, 1073–1083, 1986.
- Hirooka, T., and I. Hirota, Normal mode Rossby waves observed in the upper stratosphere. Part II: Second antisymmetric and symmetric modes of zonal wavenumbers 1 and 2, *J. Atmos. Sci.*, **42**, 536–548, 1985.
- Hirooka, T., and I. Hirota, Further evidence of normal mode Rossby waves, *Pure Appl. Geophys.*, **130**, 277–289, 1989.
- Hirota, I., and J. Barnett, Planetary waves in the winter mesosphere - preliminary analysis of Nimbus 6 PMR results, *Q. J. R. Meteorol. Soc.*, **103**, 487–498, 1977.
- Hirota, I., and T. Hirooka, Normal mode Rossby waves observed in the upper stratosphere. Part I: First symmetric modes of zonal wavenumbers 1 and 2, *J. Atmos. Sci.*, **41**, 1253–1267, 1984.
- Hitchman, M. H., J. C. Gille, C. D. Rodgers, and G. Brasseur, The separated polar winter stratopause: A gravity wave driven feature, *J. Atmos. Sci.*, **46**, 410–422, 1989.
- Kanzawa, H., Warm stratopause in the Antarctic winter, *J. Atmos. Sci.*, **46**, 435–438, 1989.
- Kasahara, A., Effect of zonal flows on the free oscillations of a barotropic atmosphere, *J. Atmos. Sci.*, **37**, 917–929, 1980.
- Labitzke, K., The interaction between stratosphere and mesosphere in winter, *J. Atmos. Sci.*, **29**, 1395–1399, 1972.
- Labitzke, K., and J. J. Barnett, Review of the radiance distribution in the upper mesosphere as observed from the Nimbus 6 pressure modulator radiometer (PMR), *Planet. Space Sci.*, **29**, 673–685, 1981.
- Labitzke, K., K. Petzoldt, B. Naujokat, E. Klinker, and R. Lenschow, 25 years of the “Berlin Phenomenon” (a major warming in December 1976-January 1977), in *Collection of Reports on the Stratospheric Circulation During the Winters 1974/75-1991/92*, edited by B. Naujokat, and K. Labitzke, pp. 22–35. Solar Terrestrial Energy Program, Univ. of Ill., Urbana, 1993.
- Lait, L. R., and J. L. Stanford, Fast, long-lived features in the polar-stratosphere, *J. Atmos. Sci.*, **45**, 3800–3809, 1988.
- Lawrence, B. N., G. J. Fraser, R. A. Vincent, and A. Phillips, The 4-day wave in the Antarctic mesosphere, *J. Geophys. Res.*, **100**, 18,899–18,908, 1995.
- Leovy, C., and T. Ackerman, Evidence for high-frequency synoptic disturbances near the stratopause, *J. Atmos. Sci.*, **30**, 930–942, 1973.
- Madden, R. A., Observations of large-scale traveling Rossby waves, *Geophys. Res.*, **17**, 1935–1949, 1979.
- Manney, G. L., The stratospheric 4-day wave in NMC data, *J. Atmos. Sci.*, **48**, 1798–1811, 1991.
- Manney, G. L., and W. J. Randel, Instability at the winter stratopause, a mechanism for the 4-day wave, *J. Atmos. Sci.*, **50**, 3928–3938, 1993.
- Marks, C. J., Some features of the climatology of the middle atmosphere revealed by Nimbus 5 and 6, *J. Atmos. Sci.*, **46**, 2485–2508, 1989.
- Miles, T., and W. Grose, Upper stratosphere polar jet instability in the southern hemisphere, *Geophys. Res. Lett.*, **16**, 239–242, 1989.
- Pedlosky, J., *Geophysical Fluid Dynamics*. Springer-Verlag, New York, 1979.
- Pfister, L., Baroclinic instability of easterly jets with applications to the summer mesosphere, *J. Atmos. Sci.*, **42**, 313–330, 1985.
- Pierce, R. B., W. T. Blackshear, T. D. A. Fairlie, W. L. Grose, and R. E. Turner, The interaction of radiative and dynamical processes during a simulated sudden warming, *J. Atmos. Sci.*, **50**, 3829–3851, 1993.
- Prata, A., The 4-day wave, *J. Atmos. Sci.*, **41**, 150–155, 1984.
- Prata, A., Observations of the 5-day wave in the stratosphere and mesosphere, *J. Atmos. Sci.*, **46**, 2473–2477, 1989.
- Randel, W. J., Global atmospheric circulation statistics, 1000-1 mb, Tech. Rep. TN-366+STR, Nat. Cent. for Atmos. Res., Boulder, Colo., 1992.
- Randel, W. J., Global normal-mode Rossby waves observed in stratospheric ozone data, *J. Atmos. Sci.*, **50**, 406–420, 1993a.
- Randel, W. J., Global variations of zonal mean ozone during stratospheric warming events, *J. Atmos. Sci.*, **50**, 3308–3321, 1993b.
- Randel, W. J., and L. R. Lait, Dynamics of the 4-day wave in the southern hemisphere polar stratosphere, *J. Atmos. Sci.*, **48**, 2496–2508, 1991.
- Rodgers, C. D., Evidence for the five-day wave in the upper atmosphere, *J. Atmos. Sci.*, **33**, 710–711, 1976.
- Rosier, S., B. Lawrence, D. Andrews, and F. Taylor, Dynamical evolution of the northern stratosphere in early winter 1991/92, as observed by the improved stratospheric and mesospheric sounder, *J. Atmos. Sci.*, **51**, 2783–2799, 1994.
- Salby, M. L., Rossby normal modes in nonuniform background configurations. Part II: Equinox and solstice conditions, *J. Atmos. Sci.*, **38**, 1827–1840, 1981.
- Schoeberl, M. R., and J. H. E. Clark, Resonant planetary waves in a spherical atmosphere, *J. Atmos. Sci.*, **37**, 20–28, 1980.
- Smith, A. K., Longitudinal variations in mesospheric winds: Evidence for gravity-wave filtering by planetary-waves, *J. Atmos. Sci.*, **53**, 1156–1173, 1996.
- Venne, D. E., Normal-mode Rossby waves observed in the wavenumber 1-5 geopotential fields of the stratosphere and troposphere, *J. Atmos. Sci.*, **46**, 1042–1056, 1989.
- Venne, D. E., and J. L. Stanford, Observation of a 4-day temperature wave in the polar winter stratosphere, *J. Atmos. Sci.*, **36**, 2016–2019, 1979.

B. N. Lawrence, Department of Physics and Astronomy, University of Canterbury, Private Bag 4800, Christchurch, New Zealand (email: b.lawrence@phys.canterbury.ac.nz)

W. J. Randel, Atmospheric Chemistry Division, NCAR, Boulder, CO 80307-3000.

(Received October 16, 1995; revised May 14, 1996; accepted May 14, 1996.)